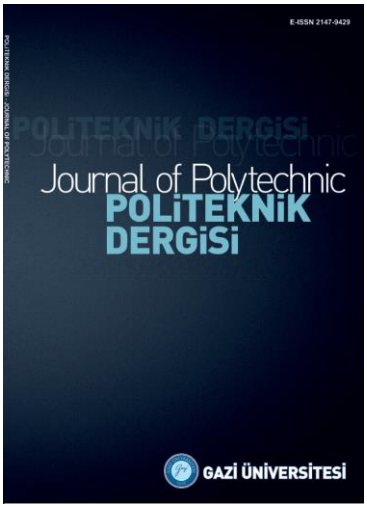

POLİTEKNİK DERGİSİ

JOURNAL of POLYTECHNIC

ISSN: 1302-0900 (PRINT), ISSN: 2147-9429 (ONLINE)
URL: http://dergipark.org.tr/politeknik

Mimicking bone anisotropic structure with modified gyroid scaffolds; a finite element analysis

Kemiğin izotropik olmayan yapısının modifiye olmuş gyroid iskelelerle taklidi; bir sonlu eleman analizi

***Yazar(lar) (Author(s))**: Daver ALİ*

ORCID: 0000-0002-8500-7820

Bu makaleye şu şekilde atıfta bulunabilirsiniz(To cite to this article): Ali D, "Mimicking bone anisotropic structure with modified gyroid scaffolds; a finite element analysis", ***Politeknik Dergisi***, 24(4): 1637-1646, (2021).

Erişim linki (To link to this article): http://dergipark.org.tr/politeknik/archive

DOI: **10.2339/politeknik.941106**

Mimicking Bone Anisotropic Structure with Modified Gyroid Scaffolds; A Finite Element Analysis

Kemiğin Izotropik Olmayan Yapısının Modifiye Olmuş Gyroid Iskelelerle Taklidi; Bir Sonlu Eleman Analizi

Highlights

- *Scaffolds with anisotropic mechanical and biological properties were designed.*
- *Anisotropic models showed different permeability in longitudinal to transverse.*
- *Gyroid architecture is a good candidate to design anisotropic scaffolds for bone tissue.*

Graphical Abstract

Deformation in the structure of the gyroid architecture caused differences in stiffness and permeability characteristics in the longitudinal and lateral directions.

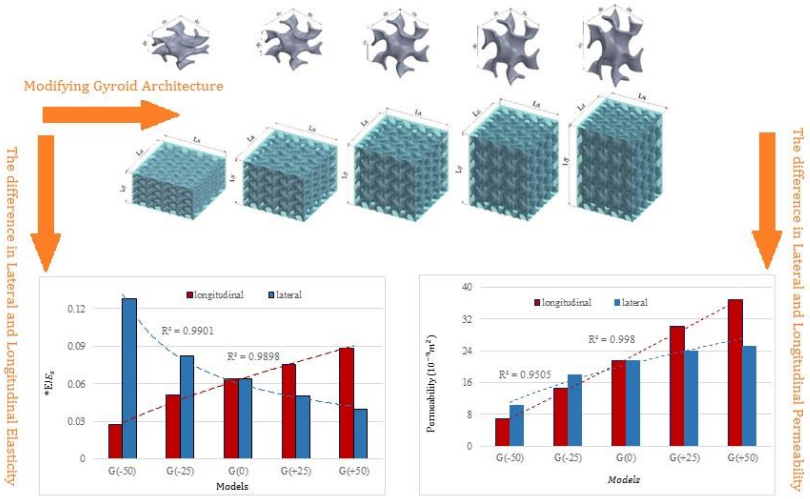

Aim

The design of implants that match the host bone anisotropic structure is necessary to maximize compliance with it.

Design & Methodology

In this study, a gyroid structure that generally is used in bone scaffolds was modified to design anisotropic scaffolds.

Originality

In this study, for the first time, gyroid architecture has been used to design tissue scaffolds with anisotropic elastic and permeability properties.

Findings

By modifying the gyroid architecture, scaffolds with non-isotropic characteristics were designed simultaneously in terms of both stiffness and permeability.

Conclusion

The result of this study showed with anisotropic gyroid structure the desired anisotropic properties in bone scaffolds can be obtained.

Declaration of Ethical Standards

The author of this article declare that the materials and methods used in this study do not require ethical committee permission and/or legal-special permission.

Mimicking Bone Anisotropic Structure with Modified Gyroid Scaffolds; A Finite Element Analysis

Research Article

Daver ALİ*

Karabuk University, Faculty of Engineering, Department of Medical Engineering, Karabuk, Turkey

(Received : 22.05.2021 ; Accepted : 17.08.2021 ; Early View : 06.09.2021)

ABSTRACT

The structure of the bone is very complex and heterogeneous; this causes different mechanical and biological properties in its longitudinal and transverse directions. For example, the modulus of elasticity and the permeability of the trabecular bone in a longitudinal and radial direction can vary up to several times. Therefore, implant design that matches these differences is necessary to maximize compliance with the host bone. Given that, in this study, a gyroid structure that generally is used in bone scaffolds was modified to design anisotropic scaffolds. Therefore, the gyroid triply periodic minimal surface trigonometric function was manipulated, and five different architectures were denoted as G(-50), G(-25), G(0), G(+25), and G(+50) with a constant porosity of 80% were developed. The effective elastic moduli of the models were calculated using finite element analysis. The results showed an anisotropicity rate of 0.21, 0.62, 1.50 and 2.23 in elastic moduli for G(-50), G(-25), G(+25) and G(+50) models respectively. As well, the permeability of the models was calculated using computational fluid dynamics (CFD) analysis. Anisotropic models showed different permeability in longitudinal and transverse directions. Longitudinal permeability to lateral direction rate were 0.67, 0.80, 1.25 and 1.47 for G(-50), G(-25), G(+25) and G(+50) models respectively.

Keywords: Anisotropic scaffolds, TPMS scaffolds, gyroid, bone elasticity, permeability.

Kemiğin İzotropik Olmayan Yapısının Modifiye Olmuş Gyroid Iskelelerle Taklidi; Bir Sonlu Eleman Analizi

ÖZ

Kemiğin yapısı karmaşık ve heterojendir, bu da boylamasına ve enine yönlerinde farklı mekanik ve biyolojik özelliklere neden olur. Örneğin, trabeküler kemiğin uzunlamasına ve enine yönde elastik modülü ve geçirgenliği birkaç kata kadar değişebilir. Dolaysıyla, implantların tasarımında konuk kemikle uyum sağlaması için bu farklılıkları dikkate almak gerekir. Bu çalışmada, yaygın olarak kemik iskeleleri tasarımında kullanılan gyroid yapısı, izotropik olmayan iskeleler modellemek için modifiye edilmiştir. Bu nedenle, gyroid üçlü periyodik minimal yüzey trigonometrik fonksiyonu manipüle edilerek ve %80 sabit bir gözenekliliğe sahip beş farklı iskele G (-50), G (-25), G (0), G (+25) ve G (+50) modeli elde edilmiştir. Modellerin etkili elastik modülleri sonlu elemanlar analizi kullanılarak hesaplanmıştır. Analiz sonuçları G (-50), G (-25), G (+25) ve G (+50) modellerin boylarınca elastisite modülünün enlerine göre sırasıyla 0.21, 0.62, 1.50 ve 2.23 oranda olduğunu göstermiştir. Ayrıca modellerin geçirgenliği hesaplamalı akışkanlar dinamiği (CFD) analizi kullanılarak hesaplanmıştır. İzotropik olmayan modeller boyuna ve enine yönlerde farklı geçirgenlik göstermiştir. G (-50), G (-25), G (+25) ve G (+50) modellerin geçirgenliği boylarınca enlerine göre oranı sırasıyla 0.67, 0.80, 1.25 ve 1.47 olarak hesaplanmıştır.

Anahtar Kelimeler: İzotropik olmayan iskeleler, TPMS iskeleler, gyroid, kemik Elastikliği, geçirgenlik.

1. INTRODUCTION

Although the bone is a tissue that can repair the damage itself, in cases where the broken parts of the bone are substantially far from each other, the use of an implant to fill this gap is inevitable [1]. The availability of spaces through implants for cell attachment, proliferation, and migration is necessary, [2] so porous scaffolds were developed [3] [4] Nowadays, the design and optimization of scaffolds for bone treatment is a critical issue in tissue engineering.

Because bone transfers loads, the scaffold that is used as a bone replacement must possess enough mechanical properties. The most crucial mechanical parameter for an implant is its' stiffness [5]. Many studies showed scaffold stiffens play the leading role in cells proliferation and differentiation within scaffolds pores [6] [7] Moreover, an excessively high stiffness can cause stress-shielding in the contact region with bone, which is an undesirable phenomenon in the implanting process [8]. Along with the mechanical properties of the implants, their biological parameters like permeability should also be considered.

Scaffolds permeability controls nutrient and gas diffusion and wastes emission during an implantation process [9]. The fluid flow-induced wall shear stress (WSS) perfusion cell culture method is the most critical factor in stimulating cells to proliferate and differentiate [10] [11]. Accordingly, the determination of fluid flow-induced WSS is also a crucial issue in scaffolds design.

*Sorumlu Yazar (Corresponding Author)
e-posta : daverali@karabuk.edu.tr

Porous scaffolds are widely used to fit implant mechanical and biological requirements [3] [4] [5] [12]. Scaffolds with high porosity are designed and constructed in various morphologies, most notably based on lattices [13] [14] and triply periodic minimal surfaces (TPMS) [15] [16]. Different architectures of scaffolds enable tissue engineers to control their mechanical properties. For example, by changing the scaffolds' porosity and geometrical parameters, their mechanical properties can be tuned [17]. Biological parameters like fluid flow-induced WSS and permeability in the scaffolds are governed by their architecture [18] [19].

Most studies in the scaffold design are based on the assumption that the bone is an anisotropic structure, and consequently, scaffolds are mainly designed as isotropic architectures [20]. In comparison, the bone is an anisotropic tissue and possesses different mechanical properties in longitudinal and transverse directions [21] [22]. Recently, Asgari et al. found differences of 10-15% and 42% in elastic moduli in longitudinal and transverse directions for cortical and trabecular bones, respectively [23]. In terms of permeability also trabecular bone behaves as an anisotropic permeable porous media [24] [25]. Some researchers have tried to produce scaffolds with anisotropic structures. For example, Ataee et al. built Ti-6Al-4V scaffolds using the electron beam melting method. Their results showed elastic modulus in the manufacturing direction was 70% higher than was in another direction [26]. Although this is a promising approach for producing scaffolds with anisotropic characteristics, it depends on the production method that limits its' applicability. In addition, in that study, they didn't clarify changes in biological parameters like permeability and fluid flow-induced WSS. Hence, the design of scaffolds that inherently are anisotropic architectures can help produce scaffolds that mimic the host bone structure [27] [28].

The experimental studies in this field need high technology and expensive facilities [29]. Instead, computer simulations in studying mechanical behaviour and biological parameters measurement of scaffolds are more cost and time-effective [30]. Nowadays, many in silico studies have been carried out to evaluate scaffolds' mechanical and biological behaviour [14] [31].

Among TPMS scaffolds, gyroid architecture with symmetric structure in all three axes, high surface area rate to volume, and high interconnectivity gained much attention in tissue engineering [32] [33]. This study used the gyroid structure to design scaffolds with anisotropic elasticity moduli and permeability in longitudinal and transverse directions with a constant porosity of 80%. For this purpose, the gyroid geometry was scaled -50, -25, +25, and +50% in only one direction, while other axes kept the same. Then, the permeability and effective elastic modulus of the models were determined using finite element analysis.

2. MATERIAL and METHOD

2.1. Scaffold Models

The K3Dsurf (k3dsurf.sourceforge.net) software was used to obtain the preliminary surfaces of the scaffolds. Trigonometric functions of $cos(x)\cdot sin(\alpha y) + cos(\alpha y)\cdot sin(z) + cos(z)\cdot sin(x) = 0$ used in designing of the gyroid scaffolds unit cell. Here, α was 1.5, 1.25, 1, 0.75 and 0.5 for scaffolds with -50% , -25% 0%, 25% and 50% scaling coefficient respectively. The models based on scaling percentage were denoted as G(-50), G(-25), (G0), G(+25), and G(+50). SolidWorks (2017) software was used to thicken surfaces to produce the desired solid models. A thickness of 200 µm was applied for the scaffolds wall that can be produced easily using additive manufacturing methods [34].

By repeating unit cells by four times in three axes (x, y, and z), a cube structure with 64 unit cells for each model was obtained. The fluid domains of the models were generated by subtracting the solid parts from an enclosing box. Unit cells of models and their geometrical parameters for both solid and fluid domains were presented in figure 1, and table 1 showed.

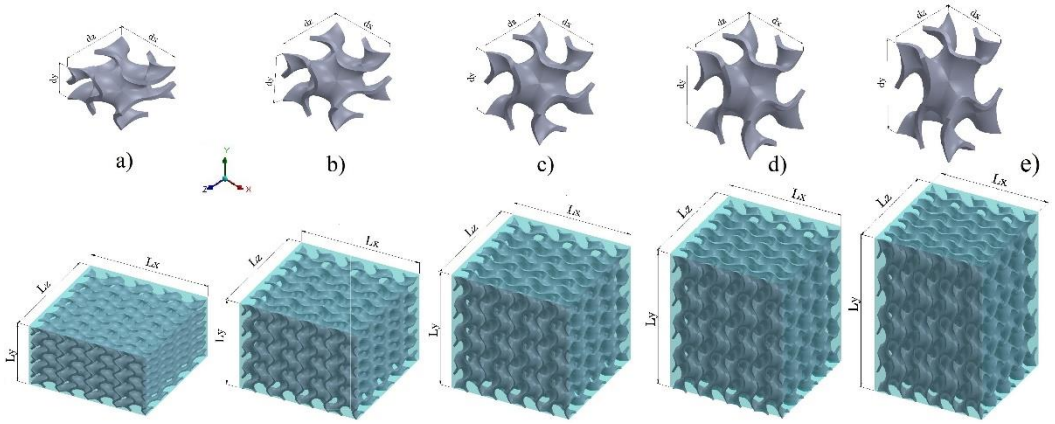

Figure. 1. Unit cells and 4x4x4 three-dimensional (3D) models of scaffolds with solid (gray) and fluid (turquoise) domains; a) G(-50), b) G(-25), c) G(0), d) G(+25) and e) G(+50).

Table 1. Unit-cells and related scaffolds dimensions (mm).

Model parameters	Unit cells and scaffolds Length in x, y, z (the size of unit-cells was calculated in the $[-\pi, \pi]$ boundary)				
	G(-50)	G(-25)	G(0)	G(+25)	G(+50)
dx and dz	3.10	3.10	3.10	3.10	3.10
dy	1.55	2.32	3.10	3.87	4.65
Lx and Lz	12.40	12.40	12.40	12.40	12.40
Ly	6.20	9.30	12.40	15.50	18.60

2.2. Scaffolds Stiffness

To measure the deformation magnitude of the models, they were compressed between two rigid plaques. The bottom plate was fixed, and from the top plate, a unidirectional pressure of 1 MPa was applied in the y-axis (Figure 2). The compression analysis of models was carried out using ANSYS software in the elastic region of the selected material. An elastic modulus of 193 GPa (E_s) and an optional Poisson ratio of 0.30 were adopted based on the mechanical properties of stainless steel 316L, which can be easily manufactured using selective laser melting technique [35]. Effective elastic moduli of the scaffolds were determined using Hooke's law (σ=εE).

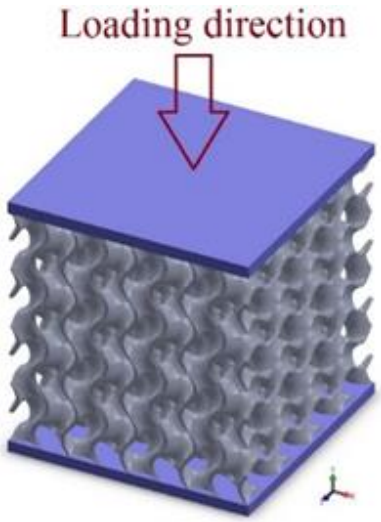

Figure 2. Using 4×4×4 of unit cells to compute the deformation in the scaffolds.

In mechanical properties analysis, the models were meshed using hexagonal elements to calculate Young's modulus. A mesh indecency analysis also was carried out for scaffolds deformation. Table 2 presents the element number for each model. It is noteworthy to note the scaffolds' lateral effective elastic modulus also was determined by compressing models in the x-axis as it was measured in the y-direction.

2.3. Governing Equations and Boundary Conditions in CFD Analysis

Permeability of models was calculated using a laminar and fully developed flow of an incompressible fluid. Also, a constant density and viscosity were selected for the analysis fluid. For solving the CFD models, the Navier-Stokes equation was used as[36]:

$$\rho \frac{\partial u}{\partial t} - \mu \nabla^2 u + \rho(u.\nabla)u + \nabla p = F, \quad \nabla.u = 0 \qquad (1)$$

where; , u, and μ denoted density (1000 kg/m3 [37]), velocity (m/s), and fluid dynamic viscosity (0.001 Pa.s) as well as ∇ and p indicated del operator and pressure (Pa) respectively. Finally, F denoted forces such as centrifugal and gravity forces, where F=0 in this case [36] [38]. Permeability (k) was measured on the basis of Darcy's law [39] as follows:

$$k = \frac{u\mu L}{\Delta P} \qquad (2)$$

where u, μ, L and ΔP show the fluid flow velocity (m⁄s), dynamic fluid viscosity (Pa.s), model length (m) and pressure drop (Pa), respectively.

The WSS, was denoted by τ_ω, is a tangent drag force that is exerted by flowing fluid on scaffolds surface and is given as [40]:

$$\tau_\omega = \mu \frac{\partial u}{\partial r} \qquad (3)$$

where u indicates the flow velocity and r shows the x-, y-, and z-directions [41].

A velocity of 0.1 mm⁄s [39] [42] was assigned to the inlet during the CFD analysis (Figure 3). A hydrophilic surface assumption for scaffolds enabled us to impose a no-slip condition on scaffolds walls, as well as zero gauge pressure was assigned on the outlet region [37, 39, 43].

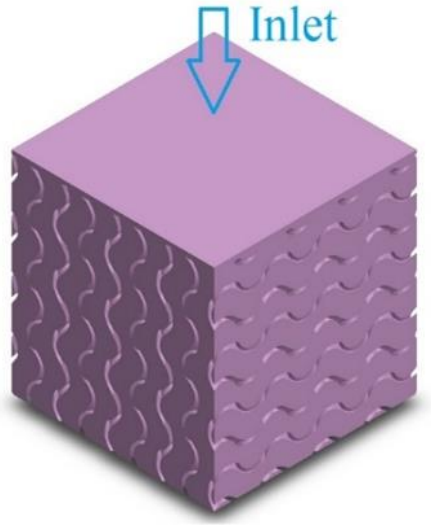

Figure 3. The fluid domain of the scaffold in CFD analysis.

Tetrahedral elements were used for meshing CFD models [18] [44]. Table 2 represents the number of elements in each model. The residual sensitivity criterion for convergence was adopted as 1e-5 [45].

Table 2. Number of elements in each model for mechanical properties analysis

Model	G(-50)	G(-25)	G(0)	G(+25)	G(+50)
Number of elements	302253	524592	637635	877384	1544037

3. RESULTS

3.1. Effective Elastic Moduli

To understand scaffolds behaviour under mechanical loading their effective elastic modulus was calculated the deformation and Hooke's law (Figure 4). The G(-50) and G(0) models showed maximum and minimum deformation respectively. Figure 5 shows a bar graph of the normalized effective elastic modulus model in both longitudinal and lateral directions.

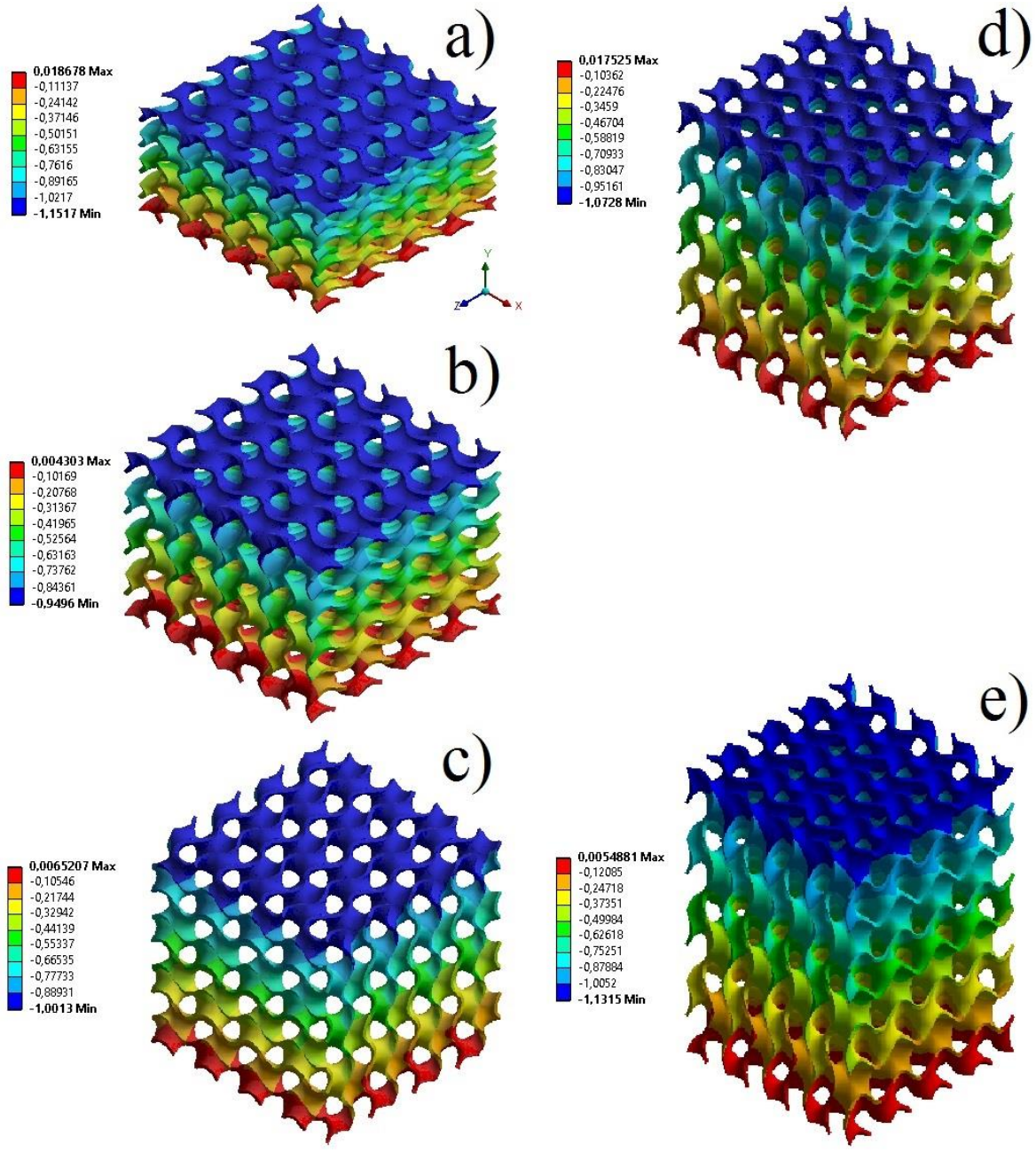

Figure 4. Deformation (µm) due to applying a pressure of 1 MPa in y-axis; a) G(-50), b) G(-25), c) G(0), d) G(+25) and e) G(+50) models.

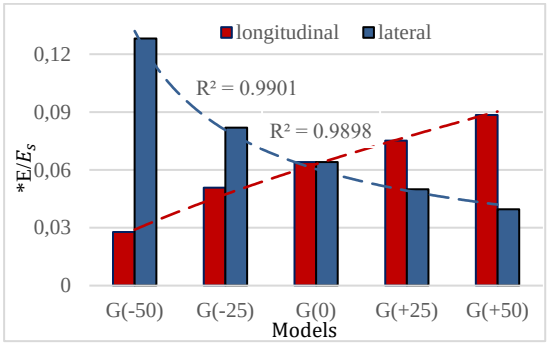

Figure 5. Longitudinal and lateral effective elastic modulus (The calculated elastic moduli were normalized with the bulk elastic modulus of 193 GPa (E_s) that was assigned to the scaffolds as basic material.

The longitudinal effective elastic moduli decreased with scaling negatively and increased when the model scaled in a positive direction. In the lateral direction, the trend of elastic modulus changes due to scaling was contrariwise to the longitudinal direction. Also, power fits curves for longitudinal and lateral directions with $R^2 = 0.99$ and 0.98 respectively showed a good correction factor between scaling coefficient and elasticity changes.

3.2. Fluid Dynamics Within Scaffolds

The fluid velocity within scaffold microchannels was variable, and in the scaffolds' center areas, its magnitude was higher than in areas were close to the wall, as shown in figure 6. Moreover, the maximum velocity in all the models is more heightened than inlet velocity, which indicates that the fluid accelerates after enters the scaffolds microchannels. This acceleration is due to the narrowing in channels and the tortuous structure of scaffolds. This phenomenon is more pronounced in the G(-50) model because its microchannels are more tortuous than are in the other models.

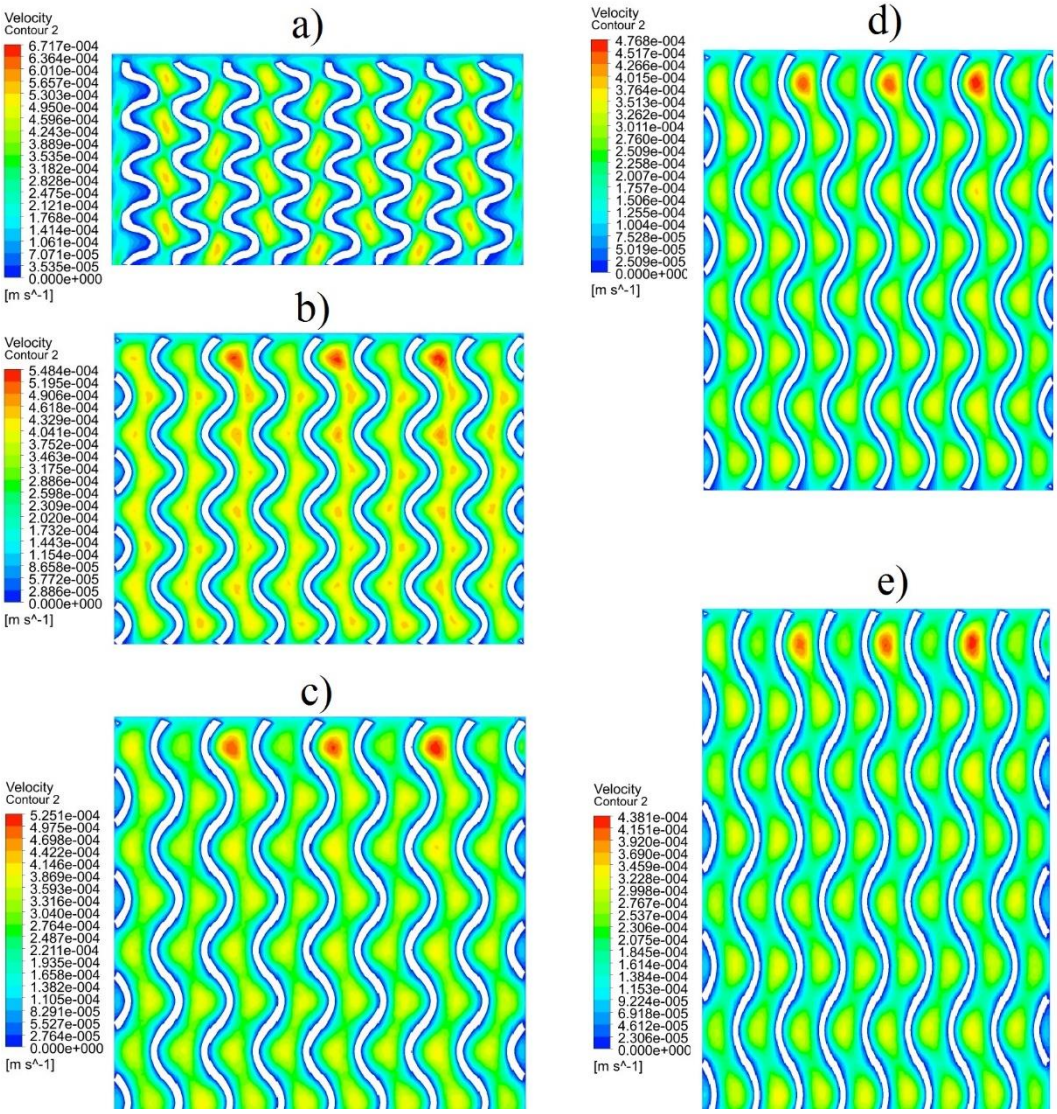

Figure 6. A velocity contour in mid-section of the models; a) G(-50), b) G(-25), c) G(0), d) G(+25) and e) G(+50) scaffolds in the longitudinal case.

3.2.1. Permeability

The permeability of each model was calculated regarding the average ΔP at the inlet measured in the CFD analysis and using Darcy's law (equation (2)). Figure 7 shows the measured permeability values for each scaffold.

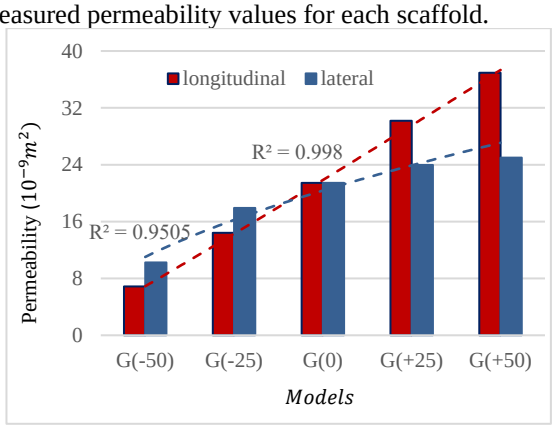

Figure 7. Darcian permeability of each scaffold.

The permeability diminished when the model was scaled negatively and enhanced when the model graduated positively for both longitudinal and lateral cases.

Moreover, the power fits curve for longitudinal with showed a good correction factor between scaling and permeability magnitudes. But for lateral direction, such a correlation could not be found.

3.2.2. WSS

The effect of change in scaffolds architecture on WSS magnitude was calculated using CFD analysis. The distribution of WSS in the scaffolds was plotted in figure 8 for the longitudinal fluid flow cases. WSS contours within the scaffolds indicate that its magnitude in different areas varies from zero to a few mPa. The maximum WSS in G(-50) model was the highest, and in G(+50) model, it was the lowest.

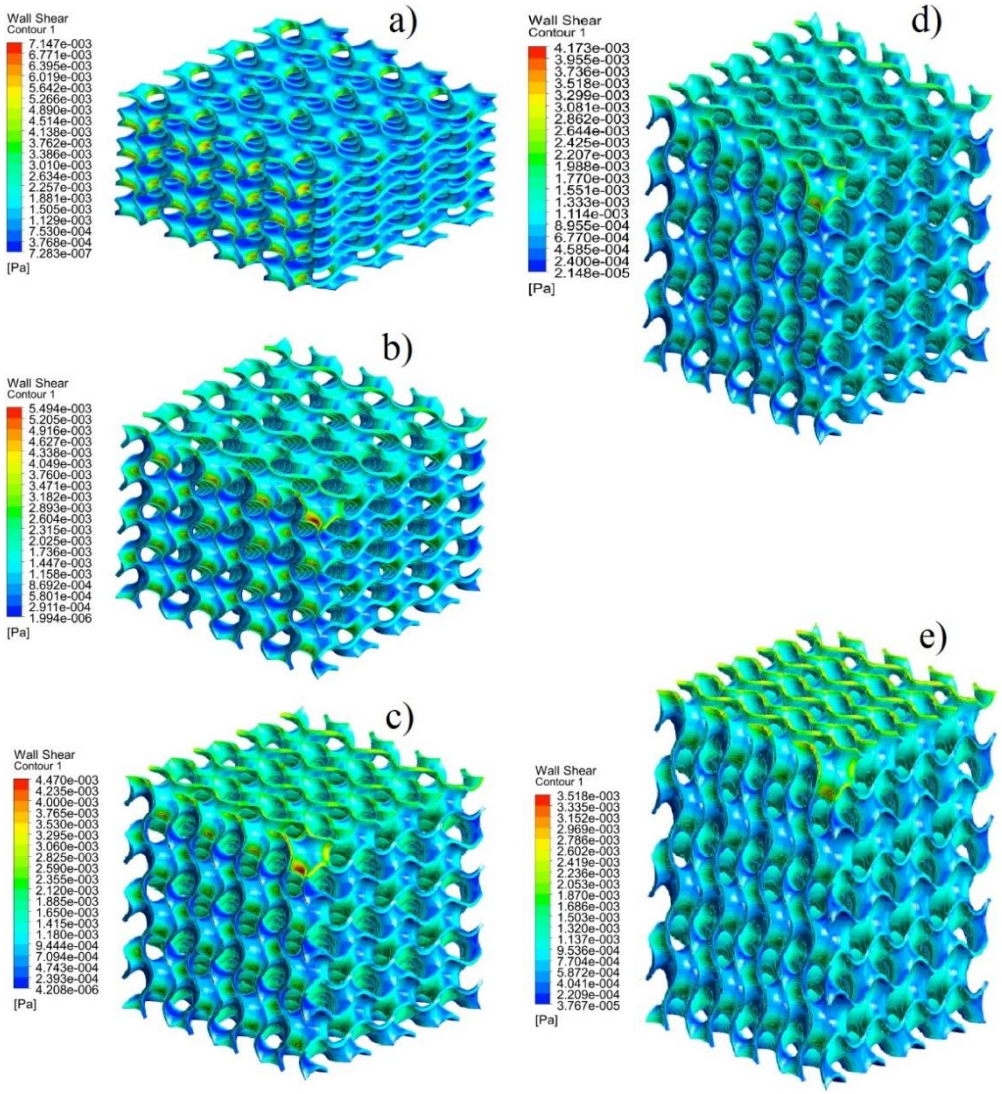

Figure 8. WSS contours for longitudinal case of the; a) G(-50), b) G(-25), c) G(0), d) G(+25) and e) G(+50) models.

Figure 9 shows a bar graph of the WSS average value for each model in the longitudinal and lateral directions.

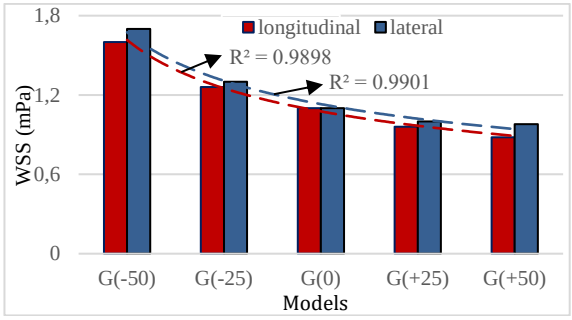

Figure 9. Mean value of WSS in both longitudinal and lateral cases for an inlet velocity of 0.0001 m/s.

The mean WSS increased with scaling in the negative direction raised and decreased when the model has scaled positively for both longitudinal and lateral cases. For both positively and negatively scaled models, WSS in the lateral direction was slightly higher than was in the longitudinal direction. Moreover, power fits curves for longitudinal and lateral directions with $R^2 = 0.98$ and 0.99 showed good correction factors between scaling percentage and average WSS variation.

4. DISCUSSION

4.1. Validity of the Results

To understand the reliability and accuracy of the results, the modulus of elasticity and permeability calculated for model G(0) in this study were compared with the results available in the literature (Table 4). As shown in table 4, both elastic modulus and permeability calculated in this study are in good agreement with the results of similar works.

Table 4. Comparison of the results for effective elastic modulus and permeability with other studies results

Model G(0)	Current study	Other works	Deviation (%)
$* E/E_s$	0.0641	0.0577 [46] 0.0638 [47]	10.00 0.37
Normalized permeability	21.45	18.43* [48]	16.38

*In that study, they normalized the calculated permeability with an empty channel (100% porosity). The permeability for such an open channel was calculated as 3036 $10^{-9}m^2$ using CFD analysis.

4.2. Elasticity behaviour of models

The increase in the modulus of elasticity in G(+25) and G(+50) models in the longitudinal direction can be because in these models, the walls of the sinusoidal structure were more moderately curved and, as a result, can be deformed hardly. Elasticity decreased in the lateral direction for these models, and this is due to the availability of relatively sharp sinusoidal curves in this direction. Such reasoning can also be described for G(-50) and G(-25) models elasticity in both longitudinal and transverse directions.

Cancellous bone is a highly porous, heterogeneous, and anisotropic material that can be seen at the epiphyses of long bones. Its elasticity depends on the bones type; patient sex and age can be very variable. For example, the Young modulus of human vertebrae was reported as 5.7±1.6 GPa; its value was calculated as 21.8 ± 2.9 GPa for the femoral head in the literature [49]. Therefore, it can be concluded that depends on the type and condition of a patient's bone; a particular implant should be provided. With this background, let's assume that a bone with an elastic modulus of 2/1 ratio in the longitudinal and transverse direction [21] needs an implant. As shown in figure 5, the G(+50) model can almost match such anisotropic elasticity.

4.3. Permeability

Because permeability is in a contrariwise relation with the pressure drop (ΔP) then it can be concluded that the permeability decreases with the increase of scaffolds resistance to the fluid flow. In the negatively scaled models, because of the reduction in pores size, the fluid flow is difficult to cross, and this increases the difference in pressure between the inlet and the outlet, resulting in low permeability. As well, the increased permeability in positively scaled models can be justified with similar reasoning.

In terms of the consistency of the models for the anisotropic permeability of bone, let's evaluate the case with an example. NAUMAN et al. reported a 12.8 and $5.49 \times 10^{-9}\, m^2$ and of permeability for human vertebral cancellous bone in longitudinal and transverse directions, respectively [50]. No one of the current study models cannot fit such an anisotropic permeability perfectly. However, model G(-50) with the condition of using in the transverse direction can meet such permeability requirement for such a bone in both directional with only 25% of deviation.

4.4. WSS

Calculated WSS (Figure 9) shows no significant difference in any of the models between the longitudinal and lateral directions. Nevertheless, the reason for reverse trends in negatively and positively scaled cases can be that, in the case of negatively scaling models, the microchannels of the scaffolds become tighter, and this causes an acceleration in fluid flow (Figure 6) and consequently caused an increase in WSS (Equation 2). For positively scaled models, an inverse state can be explained.

Finally, the results of this study showed it would be possible to imagine an individual scenario for selecting the most mimics scaffold in the bones.

5. CONCLUSION

In this study, the anisotropic scaffolds were developed using gyroid minimal surface to produce implants with varying mechanical and biological properties in different directions. The following conclusions can be drawn considering the results of this theoretical work:

- It was shown that the gyroid structure could potentially be an excellent candidate to develop anisotropic scaffolds.

- In a constant porosity, the elasticity and permeability of a gyroid scaffold can vary several times in longitudinal and transverse directions by only a few percentages scaling in one axis.
- Considering a perfusion bioreactor system for cell culture, WSS was also calculated for the anisotropic scaffolds, and no significant difference was found in longitudinal and lateral directions.
- Although the results of this study were promising for designing inherently anisotropic scaffolds, more analysis and architectures should be examined with theoretical and experimental studies.

DECLARATION OF ETHICAL STANDARDS

The author of this article declare that the materials and methods used in this study do not require ethical committee permission and/or legal-special permission.

AUTHORS' CONTRIBUTIONS

Daver ALİ: Designed the models, analyze the results, and wrote the article.

CONFLICT OF INTEREST

There is no conflict of interest in this study.

REFERENCES

[1] S. Bose, S. Vahabzadeh, and A. Bandyopadhyay, "Bone tissue engineering using 3D printing," ***Materials Today***, 16: 496-504, (2013).

[2] C. M. Murphy, M. G. Haugh, and F. J. O'Brien, "The effect of mean pore size on cell attachment, proliferation and migration in collagen-glycosaminoglycan scaffolds for bone tissue engineering," ***Biomaterials***, 31: 461-466, (2010).

[3] S. Wu, X. Liu, K. W. K. Yeung, C. Liu, and X. Yang, "Biomimetic porous scaffolds for bone tissue engineering," ***Materials Science and Engineering: R: Reports***, 80: 1-36, (2014).

[4] K. Bari and A. Arjunan, "Extra low interstitial titanium based fully porous morphological bone scaffolds manufactured using selective laser melting," ***Journal of the Mechanical Behavior of Biomedical Materials***, 95: 1-12, (2019).

[5] C. Torres-Sanchez, J. McLaughlin, and A. Fotticchia, "Porosity and pore size effect on the properties of sintered Ti35Nb4Sn alloy scaffolds and their suitability for tissue engineering applications," ***Journal of Alloys and Compounds***, 731: 189-199, (2018).

[6] C. Vyas, G. Ates, E. Aslan, J. Hart, B. Huang, and P. Barto, "Three-Dimensional Printing and Electrospinning Dual-Scale Polycaprolactone Scaffolds with Low-Density and Oriented Fibers to Promote Cell Alignment," ***3d Printing and Additive Manufacturing***, 7: 105-113 (2020).

[7] M. J. Osmond, M. D. Krebs, and M. B. Pantcheva, "Human trabecular meshwork cell behavior is influenced by collagen scaffold pore architecture and glycosaminoglycan composition," ***Biotechnology and Bioengineering***, 117: 3150-3159 (2020).

[8] J. Parthasarathy, B. Starly, S. Raman, and A. Christensen, "Mechanical evaluation of porous titanium (Ti6Al4V) structures with electron beam melting (EBM)," ***Journal of the Mechanical Behavior of Biomedical Materials***, 3: 249-259, (2010).

[9] Serpooshan, V., M. Julien, O. Nguyen, H. Wang, A. Li, N. Muja, J. E. Henderson and S. N. Nazhat, "Reduced hydraulic permeability of three-dimensional collagen scaffolds attenuates gel contraction and promotes the growth and differentiation of mesenchymal stem cells," ***Acta Biomaterialia***, 6: 3978-3987 (2010).

[10] Y. Guyot, F. P. Luyten, J. Schrooten, I. Papantoniou, and L. Geris, "A three-dimensional computational fluid dynamics model of shear stress distribution during neotissue growth in a perfusion bioreactor," ***Biotechnology and Bioengineering***, 112: 2591-2600, (2015).

[11] Y. Guyot, I. Papantoniou, F. P. Luyten, and L. Geris, "Coupling curvature-dependent and shear stress-stimulated neotissue growth in dynamic bioreactor cultures: a 3D computational model of a complete scaffold," ***Biomechanics and Modeling in Mechanobiology***, 15: 169-180, (2016).

[12] Ó. L. Rodríguez-Montaño, C. J. Cortés-Rodríguez, A. E. Uva, M. Fiorentino, M. Gattullo, G. Monno, *et al.*, "Comparison of the mechanobiological performance of bone tissue scaffolds based on different unit cell geometries," ***Journal of the Mechanical Behavior of Biomedical Materials***, 83: 28-45, (2018).

[13] V. Weißmann, R. Bader, H. Hansmann, and N. Laufer, "Influence of the structural orientation on the mechanical properties of selective laser melted Ti6Al4V open-porous scaffolds," ***Materials & Design***, 95: 188-197, (2016).

[14] P. F. Egan, V. C. Gonella, M. Engensperger, S. J. Ferguson, and K. Shea, "Computationally designed lattices with tuned properties for tissue engineering using 3D printing," ***Plos One***, 12: 1-20, (2017).

[15] S. C. Kapfer, S. T. Hyde, K. Mecke, C. H. Arns, and G. E. Schröder-Turk, "Minimal surface scaffold designs for tissue engineering," ***Biomaterials***, 32: 6875-6882, (2011).

[16] L. Y. Zhu, L. Li, Z. A. Li, J. P. Shi, W. L. Tang, J. Q. Yang, *et al.*, "Design and biomechanical characteristics of porous meniscal implant structures using triply periodic minimal surfaces," ***Journal of Translational Medicine***, 17: 1-10, (2019).

[17] C. Yan, L. Hao, A. Hussein, and P. Young, "Ti–6Al–4V triply periodic minimal surface structures for bone implants fabricated via selective laser melting," ***Journal of the Mechanical Behavior of Biomedical Materials***, 51: 61-73, (2015).

[18] S. Gómez, M. D. Vlad, J. López, and E. Fernández, "Design and properties of 3D scaffolds for bone tissue engineering," ***Acta Biomaterialia***, 42: 341-350, (2016).

[19] Zhu, Y. L., R. Q. Zhu, J. Ma, Z. Q. Weng, Y. Wang, X. L. Shi, Y. C. Li, X. D. Yan, Z. Dong, J. K. Xu, C. Z. Tang and L. Jin., "In vitro cell proliferation evaluation of porous nano-zirconia scaffolds with different porosity for bone tissue engineering," ***Biomedical Materials,*** 10: 055009, (2015).

[20] A. Arjunan, M. Demetriou, A. Baroutaji, and C. Wang, "Mechanical performance of highly permeable laser melted Ti6Al4V bone scaffolds," ***Journal of the***

Mechanical Behavior of Biomedical Materials, 102: 103517,(2020).

[21] A. A. Abdel-Wahab, K. Alam, and V. V. Silberschmidt, "Analysis of anisotropic viscoelastoplastic properties of cortical bone tissues," ***Journal of the Mechanical Behavior of Biomedical Materials***, 4: 807-820, (2011).

[22] K. Hasegawa, C. H. Turner, and D. B. Burr, "Contribution of collagen and mineral to the elastic anisotropy of bone," ***Calcified Tissue International***, 55: 381-386, (1994).

[23] M. Asgari, J. Abi-Rafeh, G. N. Hendy, and D. Pasini, "Material anisotropy and elasticity of cortical and trabecular bone in the adult mouse femur via AFM indentation," ***Journal of the Mechanical Behavior of Biomedical Materials,*** 93: 81-92, (2019).

[24] C. Daish, R. Blanchard, K. Gulati, D. Losic, D. Findlay, D. J. E. Harvie, P.Pivonka, "Estimation of anisotropic permeability in trabecular bone based on microCT imaging and pore-scale fluid dynamics simulations," ***Bone Reports***, 6: 129-139, (2017).

[25] G. Baroud, R. Falk, M. Crookshank, S. Sponagel, and T. Steffen, "Experimental and theoretical investigation of directional permeability of human vertebral cancellous bone for cement infiltration," ***Journal of Biomechanics***, 37: 189-196, (2004).

[26] A. Ataee, Y. Li, D. Fraser, G. Song, and C. Wen, "Anisotropic Ti-6Al-4V gyroid scaffolds manufactured by electron beam melting (EBM) for bone implant applications," ***Materials & Design***, 137: 345-354, (2018).

[27] G. Falvo D'Urso Labate, F. Baino, M. Terzini, A. Audenino, C. Vitale-Brovarone, P. Segers, *R. Quarto, G. Catapano,* "Bone structural similarity score: a multiparametric tool to match properties of biomimetic bone substitutes with their target tissues," ***J Appl Biomater Funct Mater***, 14: 277-289, (2016).

[28] G. F. D. Labate, G. Catapano, C. Vitale-Brovarone, and F. Baino, "Quantifying the micro-architectural similarity of bioceramic scaffolds to bone," ***Ceramics International***, 43: 9443-9450, (2017).

[29] X. Wang, S. Xu, S. Zhou, W. Xu, M. Leary, P. Choong, *M. Qian, M. Brandt, M. Xie*, "Topological design and additive manufacturing of porous metals for bone scaffolds and orthopaedic implants: A review," ***Biomaterials***, 83: 127-141, (2016).

[30] D. Ali, M. Ozalp, S. B. Blanquer, and S. Onel, "Permeability and fluid flow-induced wall shear stress in bone scaffolds with TPMS and lattice architectures: A CFD analysis," ***European Journal of Mechanics-B/Fluids***, 79: 376-385, (2020).

[31] D. Ali, "Effect of scaffold architecture on cell seeding efficiency: A discrete phase model CFD analysis," ***Computers in biology and medicine***, 109: 62-69, (2019).

[32] Z. Qin, G. S. Jung, M. J. Kang, and M. J. Buehler, "The mechanics and design of a lightweight three-dimensional graphene assembly," ***Science Advances***, 3: e1601536, (2017).

[33] G. S. Jung and M. J. Buehler, "Multiscale Mechanics of Triply Periodic Minimal Surfaces of Three-Dimensional Graphene Foams," ***Nano Letters***, 18 : 4845-4853, (2018).

[34] M. Burkhard, P. Fürnstahl, and M. Farshad, "Three-dimensionally printed vertebrae with different bone densities for surgical training," ***European Spine Journal***, 28: 798-806, (2019).

[35] M. Yakout, M. A. Elbestawi, and S. C. Veldhuis, "Density and mechanical properties in selective laser melting of Invar 36 and stainless steel 316L," ***Journal of Materials Processing Technology***, 266: 397-420, (2019).

[36] P. Vossenberg, G. A. Higuera, G. van Straten, C. A. van Blitterswijk, and A. J. B. van Boxtel, "Darcian permeability constant as indicator for shear stresses in regular scaffold systems for tissue engineering," ***Biomechanics and Modeling in Mechanobiology***, 8, : 499-507, (2009).

[37] A. C. Marin and D. Lacroix, "The inter-sample structural variability of regular tissue-engineered scaffolds significantly affects the micromechanical local cell environment," ***Interface Focus***, 5: 20140097, (2015).

[38] X. Xue, M. K. Patel, M. Kersaudy-Kerhoas, M. P. Y. Desmulliez, C. Bailey, and D. Topham, "Analysis of fluid separation in microfluidic T-channels," ***Applied Mathematical Modelling***, 36: 743-755, (2012).

[39] S. Truscello, G. Kerckhofs, S. Van Bael, G. Pyka, J. Schrooten, and H. Van Oosterwyck, "Prediction of permeability of regular scaffolds for skeletal tissue engineering: A combined computational and experimental study," ***Acta Biomaterialia***, 8: 1648-1658, (2012).

[40] D. Egger, M. Fischer, A. Clementi, V. Ribitsch, J. Hansmann, and C. Kasper, "Development and Characterization of a Parallelizable Perfusion Bioreactor for 3D Cell Culture," ***Bioengineering***, 4: 1-20, (2017).

[41] J. W. Gooch, "Hagen-Poiseuille Equation," in *Encyclopedic Dictionary of Polymers*, J. W. Gooch, Ed., ed New York, NY: **Springer New York,**: 355-355, (2011).

[42] R. Voronov, S. VanGordon, V. I. Sikavitsas, and D. V. Papavassiliou, "Computational modeling of flow-induced shear stresses within 3D salt-leached porous scaffolds imaged via micro-CT," ***Journal of Biomechanics***, 43: 1279-1286, (2010).

[43] A. Lesman, Y. Blinder, and S. Levenberg, "Modeling of Flow-Induced Shear Stress Applied on 3D Cellular Scaffolds: Implications for Vascular Tissue Engineering," ***Biotechnology and Bioengineering***, 105: 645-654, (2010).

[44] S. Sohrabi, J. D. Zheng, E. A. Finol, and Y. L. Liu, "Numerical Simulation of Particle Transport and Deposition in the Pulmonary Vasculature," ***Journal of Biomechanical Engineering-Transactions of the Asme***, 136: 1-11 (2014).

[45] D. Ali and S. Sen, "Finite element analysis of mechanical behavior, permeability and fluid induced wall shear stress of high porosity scaffolds with gyroid and lattice-based architectures," ***Journal of the mechanical behavior of biomedical materials***, 75: 262-270, (2017).

[46] D. W. Abueidda, R. K. Abu Al-Rub, A. S. Dalaq, D.-W. Lee, K. A. Khan, and I. Jasiuk, "Effective conductivities and elastic moduli of novel foams with triply periodic minimal surfaces," ***Mechanics of Materials***, 95: 102-115, (2016).

[47] S. Vijayavenkataraman, L. Zhang, S. Zhang, J. Y. Hsi Fuh, and W. F. Lu, "Triply Periodic Minimal Surfaces

Sheet Scaffolds for Tissue Engineering Applications: An Optimization Approach toward Biomimetic Scaffold Design," ***ACS Applied Bio Materials***, 1: 259-269, (2018).

[48] M. Zhianmanesh, M. Varmazyar, and H. Montazerian, "Fluid Permeability of Graded Porosity Scaffolds Architectured with Minimal Surfaces," ***ACS Biomaterials Science & Engineering***, 5: 1228-1237, (2019).

[49] R. Oftadeh, M. Perez-Viloria, J. C. Villa-Camacho, A. Vaziri, and A. Nazarian, "Biomechanics and mechanobiology of trabecular bone: a review," ***Journal of biomechanical engineering***, 137: 0108021-01080215, (2015).

[50] E. A. Nauman, K. E. Fong, and T. M. Keaveny, "Dependence of Intertrabecular Permeability on Flow Direction and Anatomic Site," ***Annals of Biomedical Engineering***, 27: 517-524, (1999).